Influence of the Madagascar Ridge on Eddy Variability in the Agulhas Current System: A Modelling Study

Issufo Halo[1,2,3], Roshin P. Raj[4], Pierrick Penven[5], Tarron Lamont[1,2,3], Isabelle Ansorge[3], Johnny A. Johannessen[6]

[1]Oceans and Coasts Research, Department of Forestry, Fisheries and the Environment, Private Bag X4390, Cape Town, South Africa, 8000

[2]Nansen-Tutu Centre for Marine Environmental Research, Department of Oceanography, University of Cape Town, Cape Town, South Africa, 7700

[3]Department of Oceanography, University of Cape Town, Cape Town, South Africa, 7700

[4]Nansen Environmental and Remote Sensing Centre, and Bjerknes Center for Climate Research, Bergen, Norway

[5]Univ. Brest, CNRS, IRD, Ifremer, Laboratoire d'Oceánographie Physique et Spatiale (LOPS), IUEM, 29280, Brest, France

[6]Nansen Environmental and Remote Sensing Centre, and Geophysical Institute, University of Bergen, Bergen, Norway

Key Points:

- New insight of the eddy field south of Madagascar reveals the emergence of rings, in addition to the classic eddy types
- Madagascar Ridge is predominantly an eddy generating platform, primarily responsible for the formation of anticyclonic rings in the region
- Madagascar Ridge controls about 10 Sv of the depth integrated volume transport in the greater Agulhas Current system

Corresponding author: Issufo Halo, `ihalo@dffe.gov.za`

Abstract

A regional ocean model was used to study the influence of the Madagascar Ridge on the circulation and eddy variability in the Agulhas Current system. In the control experiment, the model was run with a realistic bathymetry, whereas in the idealized run the bathymetry was modified by flattening Madagascar Ridge. When the Ridge was suppressed, no obvious changes were observed in the large-scale circulation. However, integrated transports revealed an excess of about 10 Sv ($1 \text{ Sv} = 10^6 \text{m}^3\text{s}^{-1}$) in the recirculation of the greater Agulhas Current system. Dynamic and statistically ($p < 0.05$) significant changes were observed at the mesoscale variability. Composite analysis of the radial distribution of the eddy azimuthal velocity, surface height, and relative vorticity within the Ridge domain in the experiments revealed that the presence of the Madagascar Ridge determines the emergence of a secondary class of large anticyclonic eddy types in the region, the "Madagascar rings".

Plain Language Summary

We used a computer model to study how a big underwater seafloor ridge near Madagascar (the Madagascar Ridge) affects ocean currents and vortices (eddies) in the Southwestern Indian Ocean. We did two tests: one with the ridge as it is, and another where we smoothed it out. Smoothing the ridge didn't notably change the main ocean currents, but it did reduce significantly the number of eddies in the region south of Madagascar. When we looked more closely at these eddies, we found out that near the Madagascar Ridge, they often form a distinct second class of large counterclockwise swirling eddies (Rings). This tells us something new about how eddies happen in this area, especially because of the ridge near Madagascar.

1 Introduction

Topographic structures of the world ocean's bed are among the least studied oceanic environments. Nevertheless they are fundamental for understanding the general oceanic circulation and seawater's physical, chemical and biological properties, important for the provision of several ocean ecosystem services, with direct societal implications.

The southwest Indian Ocean (Figure 1-a) hosts one of the most complex seafloor topography of the world ocean's (Parson & Evans, 2005). It is composed by an array of several shallow oceanic ridges with nearly a meridional orientation and prominent elevation, which mostly intersects a system of zonal currents, resulting in a wide range of flow field variability across different temporal and spatial scales. In general, seamounts and ridges are considered to be sites where both eddy formation and destruction frequently occur (Royer, 1978; Herbette et al., 2003).

In recent years, growing interest to understand the oceanography, productivity, ecology and management strategies of the seamounts in the southwest Indian Ocean, has emerged (Pollard & Read, 2017; Read & Pollard, 2017; Roberts & Ternon, 2020; Roberts et al., 2020; Vianello et al., 2020a; Harris et al., 2020; Marsac et al., 2020). In this region, one prominent topographic feature is the Madagascar Ridge (Figure 1-b, -c). It has been reported that the Ridge influences the hydrography (Anilkumar et al., 2007; Vianello et al., 2020b) and hydrodynamic conditions in the area (Matano et al., 1999; Quartly et al., 2006; Siedler et al., 2009; Halo et al., 2014b; Vianello et al., 2020a). A great number of altimetry derived cyclonic and anticyclonic eddy generation sites have been observed at/ and around the Ridge, in places where the bathymetric gradients are notable (Figure 1-b). Nevertheless, it is also apparent that many transient eddies vanish on encountering the Ridge's topography (Figure 1-b).

The aim of this study is to determine the extent to which the Madagascar Ridge impacts the eddy regime and characteristics in this region. Therefore, the study addresses the question: how does the Madagascar Ridge affects the eddy variability, mean properties, and the overall circulation in the Agulhas Current system?

In Section 1.1, we highlight key features of the Madagascar Ridge (Figure 1-c), relevant for the circulation patterns. In Section 2, we present the modelling approach. The results and discussion are presented in Section 3, and the main conclusions are summarised in Section 4.

1.1 Madagascar Ridge

Madagascar Ridge lies south of the Madagascar continental shelf (its domain is highlighted by the box in Figure 1-a), between 26 - 36°S and 42 - 52°E. It has a north-south extension of about 1300 km, and a maximum width of about 600 km (Nairn & Stehli, 1982). The eastern and western flanks of the Ridge rise steeply from the seabed at about 5000 m to 2000 m, shallowing the water column over the Ridge, and blocking deep zonal flows below 3000 m between Madagascar and Mozambique Basins. Over the Ridge, isolated submerged seamounts emerge (see Figure 1-b), the Mad-Ridge at about 42.25°E, 27.5°S and the Whalter Shoals at 43.54°E, 33.12°S (Roberts et al., 2020), with the latter being the shallowest, rising up to 18 m below the sea surface.
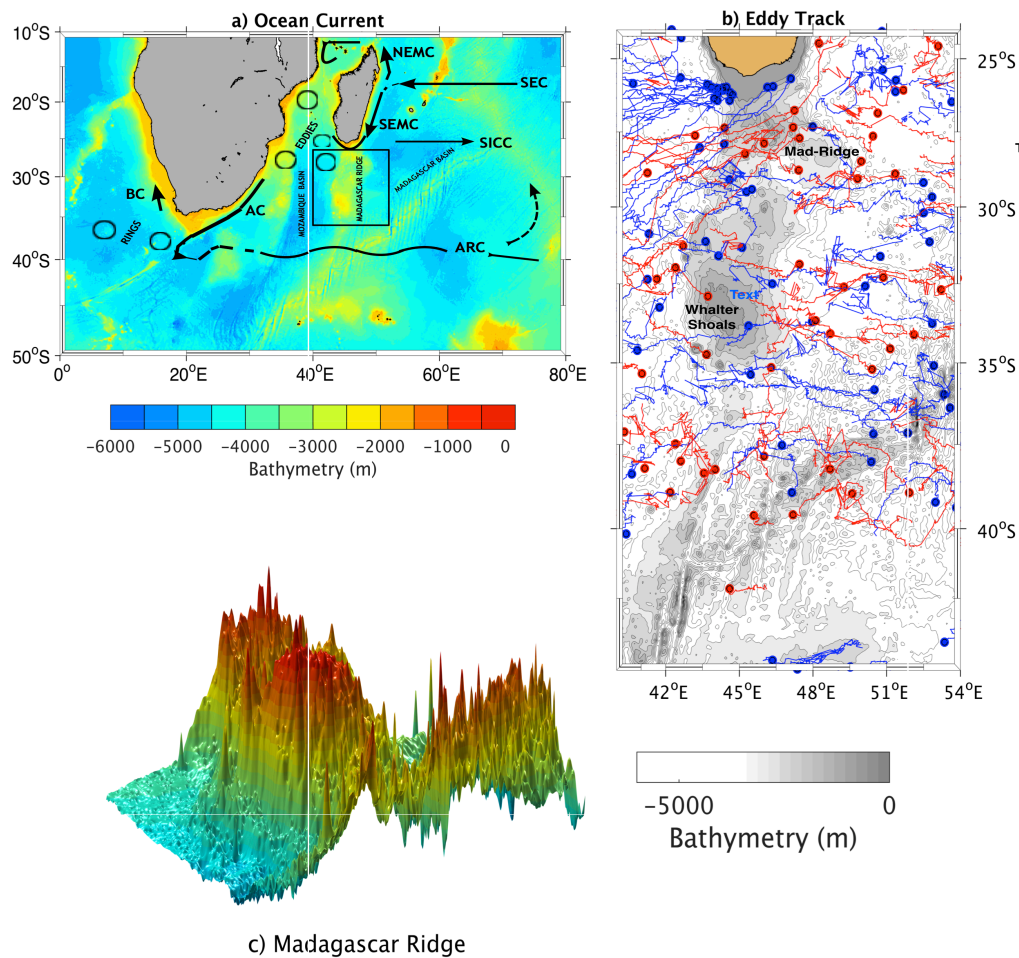
Figure 1. a) Schematic of the ocean currents overlaid seafloor topography. The Madagascar Ridge is highlighted in the overlaid square box. The main oceanographic currents are depicted, namely, South Equatorial Current (SEC), North East Madagascar Current (NEMC), South East Madagascar Current (SEMC), South Indian Counter Current (SICC), Agulhas Current (AC), Agulhas Return Current (ARC), and Benguela Current (BC). The circles represent the dominant mesoscale features, the geostrophic eddies and rings. b) Eddy Tracks, derived from satellite altimetry daily product for the years 2008 - 2009. Cyclonic eddies (blue) and anticyclonic eddies (red). The bold dots represent their generation sites and the tracks represent their propagation pathways. Only eddies with a lifetime of 60 days and longer are represented for visualization purposes. The grey shading represent the seafloor. c) The 3-dimensional view of the Madagascar Ridge is shown to highlight its morphological relief.

2 Data and Methods

2.1 Ocean model

In this study we used the Coastal and Regional Ocean Community (CROCO) model ($https://www.croco-ocean.org/$), an evolution of the former French version of the Regional Ocean Modelling System (ROMS, Shchepetkin and McWilliams (2005)).

2.1.1 Experiments Setup

The physical domain spans between 0 - 80°E, and 48 - 4°S. The bottom topography was derived from the Global Earth Bathymetric Chart of the Oceans (GEBCO) 2014 dataset. The configuration was set with 60 vertical layers, and a horizontal grid of 1/6°. Mesoscale eddies are successfully captured, the baroclinic Rossby radius of deformation in the domain ranges from about 150 km in the north to about 20 km in the south (Chelton et al., 1998).

The model was forced with monthly climatology surface wind-stress, fresh-water fluxes, heat-flux, and salt-flux, derived from the Comprehensive Ocean Atmosphere Data Sets, gridded at 1/2° (COADS05, (Da Silva et al., 1994)). To augment COADS05 winds we used wind derived from QuikScat satellite Scatterometer Climatology of Ocean Winds (SCOW) from 1999 - 2009, gridded at 1/4° (Risien & Chelton, 2008). The lateral open boundaries were derived from monthly climatology Atlas of regional seas (CARS09, $http://www.marine.csiro.au/$), gridded at 1/4° (Ridgway & Wilkin, 2002).

The model simulated the oceanic circulation under two scenarios: In the first, control run the model applied the GEBCO14 seafloor topography. In contrast, the model was run with a modified seafloor topography in the second run, characterized by an excision of the Madagascar Ridge (regarded as idealized experiment). Details of the bathymetric excision is presented in Section 2.1.2.

2.1.2 Suppressing Madagascar Ridge

The model bathymetry for the idealized experiment was reconstructed by flattening the Madagascar Ridge towards the seabed in the original GEBCO14, to a depth of about 3000 m. Subsequently the re-interpolation of the bathymetry was made using an objective analysis method to inforce a regular bathymetry shape (Penven et al., 2008). Hanning filter was applied with 15 numbers of iterations to smooth over undesirable bathymetric artefacts, in order to prevent eventual contour's discontinuities along the isobaths, which could potentially induce numerical instabilities.

Figure 2-a,b illustrates both the control and modified bathymetries respectively. A more detailed inspection of the bathymetric profiles south of Madagascar (Figure 2-b), shows the absence of the Madagascar Ridge. To ensure that the methodology used to suppress the ridge was not detrimental elsewhere away from the Ridge domain, we first performed a sensitivity test. This consisted in finding an optimal maximum depth onshore for the model parameter $hmax_{coast}$, which was then set to 200 m. This provided the best solution for the numerical difference between the control and the idealized model interpolated bathymetries (i.e, the difference with no degrading effects in areas away from the Ridge, as shown in Figure 2-c. The white areas indicate places where the bathymetry was not impacted by the excision of the Ridge, revealing that the change in bathymetry predominantly occur south of Madagascar as desired.

Under the same surface forcing, lateral open boundary conditions and initialization, the model simulations were made for 11 years, and the outputs were stored daily. The simulations reached stability after year 3 of integration. Model years 4 - 11 have then been further used in the analyses.
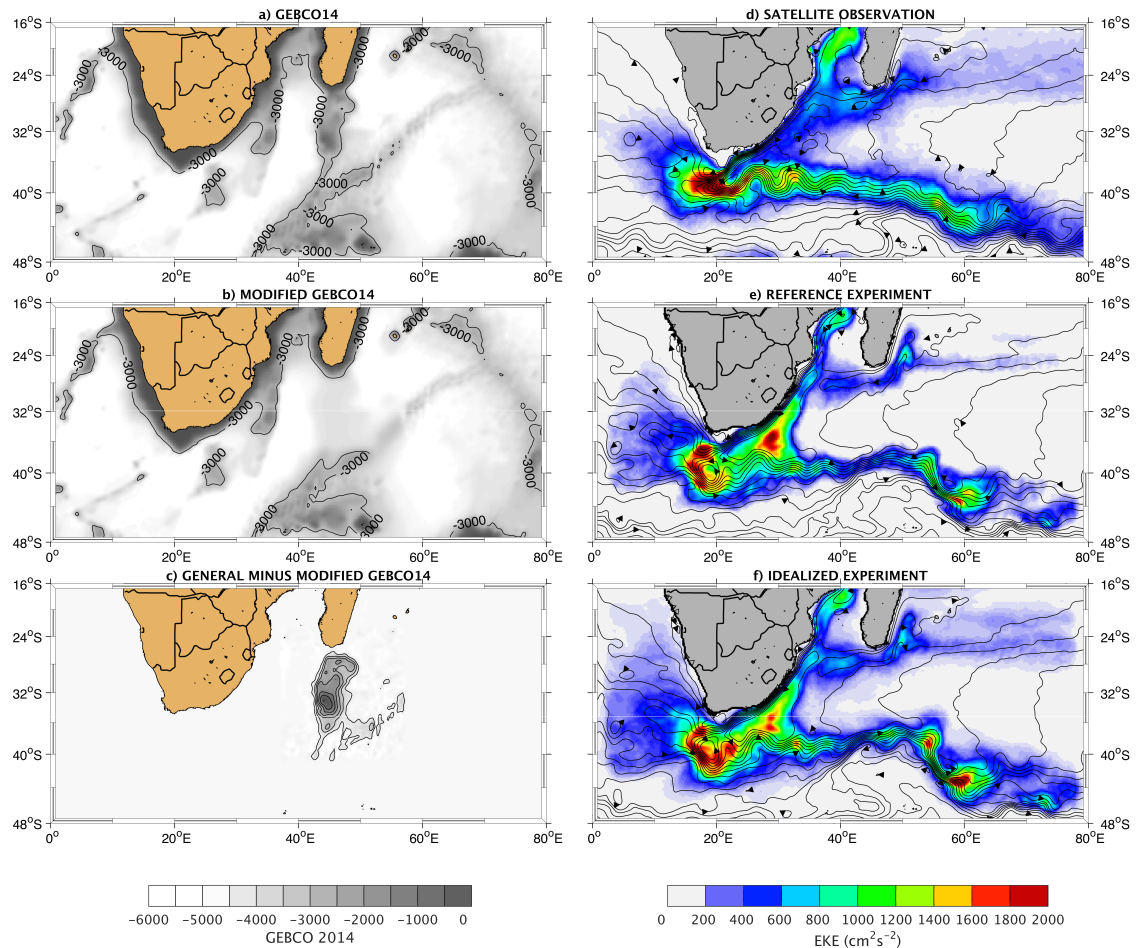
Figure 2. Left panels show seafloor topography in the Agulhas Current system, and the right panels show the EKE (colour shading) and overlaid streamlines of the mean SSH observed and simulated. a) Reference bathymetry used in the Control Experiment, and b) modified bathymetry used in the Idealized Experiment, where the Madagascar Ridge was flattened towards the seabed. c) Sensitivity test performed by subtracting the modified bathymetry from the reference bathymetry, whereby only the bathymetry around the ridge domain has been affected. d) Satellite derived EKE and mean SSH, e) EKE and mean SSH simulated in the control experiment, and f) EKE and mean SSH simulated in the modified experiment. The arrows on the streamlines show the direction of the mean flow.

2.1.3 Eddy formation

The main mechanism for eddy formation in the region south of Madagascar are the barotropic ($KmKe$) and baroclinic ($PeKe$) instabilities (De Ruijter et al., 2004; Halo et al., 2014b), defined as the transfer of energy from the mean kinetic energy to eddy kinetic energy, and from the eddy potential energy to eddy kinetic energy, respectively (Kundu, 1990; Marchesiello et al., 2003). These can be computed as:

$$KmKe = -\left[\overline{u'u'}\frac{\partial \overline{u}}{\partial x} + \overline{u'v'}\left(\frac{\partial \overline{u}}{\partial y} + \frac{\partial \overline{v}}{\partial x}\right) + \overline{v'v'}\frac{\partial \overline{v}}{\partial y}\right], \text{ and } PeKe = \overline{-\rho'w'}\frac{g}{\rho_o}.$$

In the formulas u' and v' are perturbations in time of the velocities along directions x and y respectively, and $\overline{u}$ and $\overline{v}$ are their time mean velocities. The g is the acceleration due to gravity and ρ' is the fluctuation of the seawater density, with reference density ρ_o, and w' is the fluctuation of the vertical velocities. By definition, $a'= a - \overline{a}$.

2.1.4 Eddy Detection

To identify eddies we have used the automatic eddy detection and tracking algorithm described by Halo et al. (2014a), and applied successfully in the region south of Madagascar (Halo et al., 2014b). The algorithm defines an eddy as a patch of the flow field where the relative vorticity (ζ) dominates its deformation (S), in the framework of the Okubo-Weiss parameter ($W = S^2 - \zeta^2$). Where $\zeta = \frac{\partial v}{\partial x} - \frac{\partial u}{\partial y}$, and $S^2 = S_s^2 + S_n^2$, for the normal strain $S_n = \frac{\partial u}{\partial x} - \frac{\partial v}{\partial y}$, and shear rate $S_s = \frac{\partial v}{\partial x} + \frac{\partial u}{\partial y}$ are within a closed circular strealine of the sea surface height (SSH), with radius smaller than 600 km. The tracking between consecutive timesteps is performed with reference to the eddies centers, in a generalized adimentional space frame, following the method outlined by Penven et al. (2005).

2.1.5 Eddy Composite

The methodology used to perform the eddy's composite follows the approach used by Halo et al. (2014a). Firstly we inspected histograms of the eddy density distribution per class of size to determine the nature of the distribution. Similar to Halo et al. (2014a), also the radii of the second class of anticyclonic eddy structures, appeared to emerge at 100 km. An eddy rectangular grid with an adimensional radius spanning from the eddy's origin to it's rim was defined and initialized with the eddy mean proporties. The adimentional radii was normalized by each eddy radius ($\frac{r}{R_{eddy}}$).

2.2 Altimetry Data

Satellite altimetry dataset was used to assess the mesoscale variability and evaluate the model performance. Maps of absolute dynamic topography and derived geostrophic velocities are distributed by Copernicus Marine Environmental Services (CMEMS, $https://marine.copernicus.eu/$), delivered at best two-months after the measurement. It contains level-4 SSH above the geoid, gridded at 1/4°, from a merging of all altimeter missions over the oceans (AVISO, 2015). The daily data used here spans from 1 January 1993 to 31 December 2017.

The bulk measure of mesoscale variability, the mean eddy kinetic energy was estimated as $MEKE = \frac{\overline{u'^2} + \overline{v'^2}}{2}$, where $u = -\frac{g}{f}\frac{\partial \eta}{\partial y}$, and $v = \frac{g}{f}\frac{\partial \eta}{\partial x}$, are the zonal and meridional components of geostrophic velocities respectively, g is the acceleration due to gravity, and f is the Coriolis parameter.

3 Results and Discussion

3.1 Model and Data Comparison

Maps of MEKE estimated from the satellite altimetry observations is represented by the colour shading in Figure 2-d, while the simulated control and modified experiments are represented in Figure 2-e, and Figure 2-f, respectively. The corresponding ocean surface geostrophic currents are represented by the streamlines of the mean SSH (black contours), with the direction indicated by the arrows.

To some extent the model is able to reproduce the observed spatial patterns and peak intensity of the eddy kinetic energy in the Mozambique Channel and the area south of Madagascar. The simulation also reproduced the retroflection of the Agulhas Current and the flow of the Agulhas Return Current at the right latitudinal band at 35-40°S. However, the simulations overestimate the EKE in the core of the Agulhas Current (Figure 2-e, -f), at about 30°E. Nevertheless, as both the control and modified experiments reproduced consistent large-scale patterns, the role of the Madagascar Ridge for the downstream flow field can be properly examined in these simulations.

3.2 Control versus Idealized simulations

3.2.1 Circulation and Transport

To inspect the changes in the large-scale circulation patterns between the two experiments, we have computed, mapped and compared the horizontal stream-function, (ψ) representative of the non-divergent component of the mean currents ($\vec{u}$, $\vec{v}$) vertically integrated from depth of 1500 m to the sea-surface. Following the approach used by Penven et al. (2005), the stream-function was derived from the Laplacian equation $\nabla^2\psi = (\nabla\Lambda\vec{u}).\vec{k}$, solved by enforcing an integral for mass conservation on the currents for the lateral boundary conditions. The results are shown in the left panels of Figure 3. suggesting that the pattern of the transport streamlines derived from the control and modified simulation experiments are consistent with the contours of the mean SSH presented in Figure 2-e, -f. The arrows indicate the direction of the flow, and the contour intervals between the streamlines is 10 Sv. Overall, the streamlines appears more strongly intensified in the idealized experiment (Figure 3-b) than in the control experiment (Figure 3-a), especially at the southern extension of the Southeast Madagascar Current, along the western boundary region of the Agulhas Current, and along the path of the Agulhas Return Current. This suggests a possible increase in volume transport in the idealized experiment as confirmed in the difference map seen in Figure 3-c. A positive (negative) value denotes a decreased (increased) transport in the idealized experiment.

When further inspecting Figure 3-c, a more clearer pattern emerges, evidencing an overall increase of about 10 Sv (red contours) at the southern termination of the SEMC towards the Agulhas Current. The same is true for the Agulhas Current proper and the Agulhas Return Current. However no clear evidence of an increased transport from the Indian Ocean toward the South Atlantic Ocean is observed.

This result is important as it may suggest that an increase in the transport of the Agulhas Current bears no notable impact on the transport across the Indian-Atlantic interface through the Agulhas leakage, but conversely stronger impact on the Agulhas Return Current. The relationship between the Agulhas Current and its leakage has been a subject of different interpretations: some arguing that a stronger Agulhas Current leads to a stronger leakage (Rouault et al., 2009), while others have suggested that a weaker Agulhas Current would lead to a stronger leakage (van Sebille et al., 2009a; Biastoch et al., 2009). In comparison, our results seem to corroborate the study by Loveday et al. (2014), who used ROMS model to demonstrate that the Agulhas Current leakage is independent of the local structure and transport of the Agulhas Current itself.

3.2.2 Transport variability

We have computed the timeseries of the ocean currents volume transports at four key transect lines across the South East Madagascar Current (SEMC), Agulhas Current (AC), and across the path of the Agulhas leakage (see Figure 3-a). The transports were estimated by vertically integrating the lateral fluxes across the sections.

The selection of these four geographical locations, moreover, allows comparison to in-situ observations. The transect at 23°S crosses the SEMC and offer data from a 11-month long current-meter mooring array (Schott et al., 1988). The transect across the southern extension of the SEMC at 45°E provides hydrographic data (Nauw et al., 2008). In the core of the Agulhas Current, the transect at 32°S allows comparison to the WOCE 1995 hydrographic data, and many other ventures (Beal & Bryden, 1999; Donohue et al., 2000; Donohue & Toole, 2003; Bryden et al., 2005). The transect along the Good-Hope line at 10°E in the southeast Atlantic Ocean also offer hydrographic data (Swart et al., 2008).

The middle panels in Figure 3 shows the models derived transport timeseries, while their corresponding power-spectra are presented in the right panels, computed using the multitaper spectral scheme (Thompson, 1982; Percival & Walden, 1993). The control experiment is depicted in black and idealized experiment in blue colour. The model estimates of the mean transports and their standard deviations are inserted in the panels. The poleward volume transport of the SEMC at 23°S has been estimated in various studies, providing quantities ranging from 20 to 56 Sv (Swallow et al., 1988; Schott et al., 1988; Stramma & Lutjeharms, 1997; Donohue & Toole, 2003). These variations have been attributed to different assumptions being made in relation to the uncertainties of the level of no motion, current structure and the latitudinal positions used to capture the current (Nauw et al., 2008). Our model estimates of 15.92 ± 6.97 Sv for the control run, and 18.06 ± 6.64 Sv for the idealized run (Figure 3-d) are slightly below the range estimated by the above mentioned hydrographic data. However they are slightly higher than the estimates of about 14.8 Sv simulated in general ocean circulation model (Quartly et al., 2006).

At the southern tip of Madagascar, the transect at 45°E, between 27.5°S and the continental shelf, crosses the southern termination of the SEMC, which at this point generally flows in a westward direction. Its transport receive an additional contribution from anomalies of SSH originated in the far eastern Indian Ocean (Schouten et al., 2002a; De Ruijter et al., 2004; Palastanga et al., 2006; Ridderinkhof et al., 2013), and mostly in form of mesoscale eddies (Quartly et al., 2006; Halo et al., 2014b). This may explain the increased volume transport reported in the SEMC's control experiment, from 15.92 Sv at 23°S to 22.25 Sv at 45°E, an excess of about 6.33 Sv (Figure 3-e).

When the model derived mean transports at 45°E are compared against each other, i.e, 22.25 ± 12.64 Sv from the control experiment against 29.56 ± 6.36 Sv from the idealized, it is notable an excess of about 7.31 Sv ($\sim 14\%$) in the idealized experiment (Figure 3-e). Notice that the timeseries exibit relatively lower amplitude fluctuations, which could possibly indicate lower energy levels, and less variability, especially across the mesoscale range. In fact looking at the power-spectrum a remarkable dispersion between the profiles of the control and idealized experiments were evident, characterized by a diminishing power in the idealized experiment, manifested in the frequency range of 1.5 - 5 cycles/year (Figure 3-i). This is likely related to a decay of energy at the mesoscale range as suggested by the lower standard deviation ($\sim 50\%$ decrease). Interestingly, in the control experiment the power-density for processes on the frequency range between 3 and 4 cycles/year (mesoscale) is higher than that in the annual frequency 1 cycle/year (Figure 3-e). This could indicate an upscale cascade of energy. The same can not be said for the idealized experiment as the highest peak of the power-density was limited in the annual cycle (Figure 3-i).
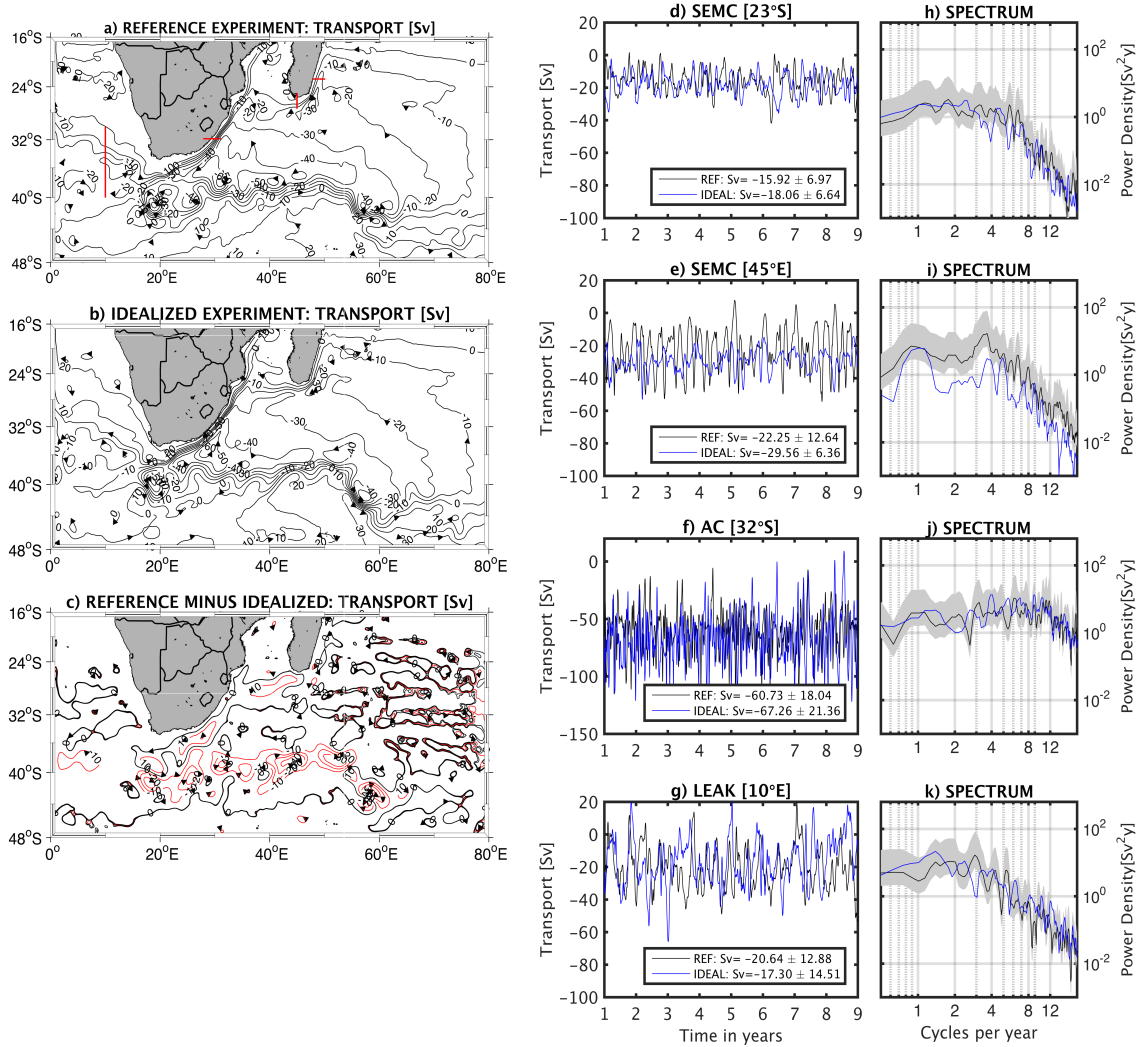
Figure 3. (Left panels) Model derived streamlines of transports in the greater Agulhas Current system. a) Control simulation, b) Idealized simulation, c) difference between the Control and Idealized experiments. The red contours highlight the 10 Sv labelled streamline, indicative of excessive transport. (middle panels) Timeseries of transport estimates across the current, at key specified transect locations marked as red lines in panel a). (right panels) Corresponding power spectra.

Therefore it is reasonable to conclude that the excision of the Madagascar Ridge partly suppress instabilities in the currents that develops when the Ridge is present.

In the core of the Agulhas Current, estimation of the volume transport at 32°S, based on hydrographic measurements have indicated transports ranging between 70 and 78 Sv (Beal & Bryden, 1999; Donohue et al., 2000; Donohue & Toole, 2003). In comparison, our model estimates were about 60.73 ± 18.04 and 67.26 ± 21.36 Sv for both control and idealized experiments respectively (Figure 3-f). The agreement is even better when compared to numerical simulation of Lagrangian floats over a 37 years time period, providing a poleward Agulhas Current mean transport of 64 Sv at 32°S (van Sebille et al., 2009a, 2009b). Note that about 6.54 Sv ($\sim 5\%$) is in excess in the idealized experiment.

The power-density spectrum profiles of the transport of the Agulhas Current have shown a declining slope (Figure 3-j) from the annual cycle (1/year) to 10 cycles/year. This is again a potential indication of an upscale cascade of energy, evident for both the control and idealized experiments. Notice that no obvious distinction between the profiles of the two experiments is evident (Figure 3-f). This could suggest that the excision of the Ridge had relatively less impact on the mesoscale variability in the core of the Agulhas Current in this region.

The same may also be said for the transport flowing into the south Atlantic (Figure 3-g). Our model estimations of the volume transports across the Good-Hope transect line at 10°E range from 20.64 Sv (control) to 17.30 Sv (idealized). These model estimates are comparable with independent estimates of the mean leakage ranging from 19.4 and 22.4 Sv (Le-Bars et al., 2014), to 17.6 Sv (van Sebille et al., 2009b). The decreased mean transport of about 3.34 Sv ($\sim 9\%$) estimated in the idealized experiment (Figure 3-g), could be related to the larger transport into the Agulhas Return Current as evidenced in Figure 3-c.

All in all, the idealized experiment generally provides relatively higher mean volume transports when compared to the control experiment. The excision of the Madagascar Ridge has facilitated a large increase of the current transports in the re-circulating branches of the subtropical anticyclonic gyre of the Southwest Indian Ocean. Moreover, the power-spectra suggest that the excision of the Madagascar Ridge has most notable localized impact on the mesoscale variability around the southern Madagascar region.

In Section 3.2.3 the impact of the Ridge excision on the mesoscale eddy field is further examined, looking at eddy occurrence, formation mechanism and mean characteristics in these two distinct regions.

3.2.3 Eddy Occurrence

The presence of eddies were searched across the whole domain, in both the control and idealized experiments, using the algorithm described in Section 2.1.4. The spatial distribution of the eddies in terms of their annual frequency of occurrence, in each grid cell of $0.5° \times 0.5°$ size, expressed in percentage (%), for the integrated period (4 - 11 years) in the greater Agulhas Current system is shown in Figure 4. The left panels (Figure 4-a, -b), present the distribution of the cyclonic and anticyclonic eddies, respectively in the control experiment, whereas the middle panels (Figure 4-c, d) present the corresponding distribution in the idealized experiment. Only the eddies with a lifetime of 30 days and greater have been considered.

Mesoscale eddies can be found almost everywhere regardless of the model experiment (Figure 4-a to -d). Comparisons between the cyclonic and anticyclonic eddy occurrences reveal highest generation rates for anticyclonic eddies (of about 5 per year), mostly located in the Mozambique Channel and south of Madagascar, as well as in vicin-

ity of the core of the Agulhas Current, in the Agulhas Retroflection and in parts of the Agulhas Return Current. These patterns of eddy occurrences are consistent with those documented in the literature, known to be generated predominantly by barotropic instabilities of the flow (Schouten et al., 2002a, 2003; De Ruijter et al., 2002; H. & De Ruijter, 2003; De Ruijter et al., 2004; Ridderinkhof et al., 2013; Halo et al., 2014a, 2014b).

When the control experiment (Figure 4-a, -b) is compared to the idealized experiment (Figure 4-c, -d), it becomes apparent that the spatial distribution of the eddy generation rates are more diffused in the idealized experiment, particularly to the south of Madagascar, where the Ridge has been removed. This may suggest that the presence of the Madagascar Ridge confines the ocean currents in particular directions, which may allow eddies to have a more consistent preferential pathway when crossing the Ridge.

To further examine the eddy generation mechanisms and their mean properties, we have defined two boxes (Figure 4-a), one covering the Madagascar Ridge domain (42 - 52°E, 37 - 27.5°S), and the other, the Agulhas Retroflection region (12 - 22°E, 44.5 - 36°S). These results are further addressed in Section 3.2.4.

3.2.4 Barotropic and Baroclinic processes

The box average profiles for barotropic (KmKe) and baroclinic (PeKe) instabilities estimated through the water column following the approach addressed in Section 2.1.3 are presented in Figure 4-e and Figure 4-f. For both panels, the profiles derived from the boxes over the Madagascar Ridge / Agulhas Retroflection area are presented in red / blue colours. Moreover, the control experiment is portrayed by the continuous lines, while the idealized experiment is portrayed by the dotted-lines. It is also important to note the different scales displayed in Figure 4-e and Figure 4-f.

Investigations of the barotropic instability processes (Figure 4-e), shows that KmKe in the Agulhas Retroflection region (blue profiles) is by far greater than in the area south of Madagascar (red profiles). This is not surprising as the energy levels in the Agulhas Retroflection region is by far greater than that south of Madagascar, as also depicted in Figure 2-d. In the latter area, the profiles of KmKe moreover show largest values confined to the upper 500 m (Figure 4-e). This would be expected as the core of the mean currents crossing the Madagascar Ridge, such as the SICC are confined in the upper 500 m (Siedler et al., 2009; Halo et al., 2014b). Hydrographic measurements collected in the area south of Madagascar presented by De Ruijter et al. (2004), suggests that by conservation of potential vorticity, the shallow bottom topography of the Madagascar Plateau in conjunction with the β-effect acting on the southwestward branch of the SEMC generates anticyclonic relative vorticity that stimulates the formation of eddies. The time-series of vertical profiles of geostrophic currents in the upper 350 m of the water column derived from seven moorings over the Madagascar Ridge (from 2011 - 2014) reveals consistent pattern of current reversals (Vianello et al., 2020a), indicative of frequent localized eddy formation.

Moreover, when the KmKe in the control experiment (continuous red profile) is compared to the idealized experiment (dotted red profile), one notice that while the profile for the control experiment deflects towards positive KmKe values, the profile for the idealized experiment deflects toward negative KmKe values. While the former is indicative of eddy formation in agreement with Halo et al. (2014b), the latter suggests that the eddies tend to vanish toward the mean flow (Marchesiello et al., 2003). This may explain why relatively fewer eddies have been found in the idealized experiment.

In comparison, the KmKe profiles in the Agulhas Retroflection region suggests eddy production in the upper 4000 m, regardless of the model experiment. Nevertheless, in both cases the largest production appears in the upper ocean surface layer (Figure 4-e).

This indicates surface and sub-surface eddy formation in the Agulhas Retroflection region.

The PeKe reveals on the other hand, more variable patterns (Figure 4-f). South of Madagascar, the energy transmission towards the eddy production are evident both at surface and sub-surface layers (~ 900 m), as previously reported by Halo et al. (2014b). In the Agulhas Retroflection region the profiles show a great deal of eddy production in the upper 500 m, while at intermediate depths, near 1000 m, peak eddy energy is converted towards the eddy potential.

3.2.5 Eddy Statistics and Size Distribution

Eddy statistics and characteristics were assessed within the two boxes where the KmKe and PeKe profiles were examined. The histograms of eddy occurrence per class of size are shown in the lower panels in Figure 4. The distribution derived from the control experiment is shown in Figure 4-g and Figure 4-h for the areas south of Madagascar and Agulhas Retroflection respectively. In comparison, the distribution derived from the idealized experiment are respectively shown in Figure 4-i and Figure 4-j.

With regards to the control experiment south of Madagascar, the most predominant eddies were centered at 50 km radius for the cyclones (dark grey), while the anticyclones (light grey) dominated radii range between 50 and 60 km (Figure 4-g). In the Agulhas Retroflection region (Figure 4-h), the most predominant cyclonic eddies were centered between 30 and 40 km, while the anticyclones centered around 40 km.

In contrast, the idealized experiment generated relatively larger cyclonic and anticyclonic eddies in the south of Madagascar area, with radii centered at 60 km (Figure 4-i). Similar results were obtained in the Agulhas Retroflection region (Figure 4-j), where the idealized experiment also generated predominant eddy sizes centered at 40 km radii, for both cyclonic and anticyclonic eddies.

The decreasing dominant eddy sizes from the Madagascar Ridge domain to the Agulhas Retroflection region observed in both simulation experiments is consistent with f-plane induced decrease in the Rossby radius of deformation from the area south of Madagascar southward to the Agulhas Retroflection region (Chelton et al., 1998).

We also determined the overall eddy mean diameters (L) in both experiments. The control experiment south of Madagascar produced cyclones with $L = 117.14 \pm 20.55$ km, and anticyclones with $L = 142.67 \pm 28.65$ km. In comparison, the idealized experiment produced cyclones with $L = 123.73 \pm 30.54$ km, and anticyclones with $L = 134 \pm 46.19$ km. The statistic indepedent $t - test$ for the difference between the mean values (cyclones vs anticyclones) was significant ($p < 0.05$), only in the control experiment.

In the Agulhas Retroflection region, the control experiment produced cyclonic eddies with an overall $L = 127.35 \pm 23.87$ km, and the anticyclonics with $L = 147.57 \pm 47.69$ km. The idealized experiment on the other hand produced a mean size of cyclonic eddies with $L = 122.87 \pm 25.94$ km, and anticyclonic eddies with $L = 147.45 \pm 55.46$ km. These mean values indicate no significant difference between the experiments, for the Agulhas Retroflection area.

3.2.6 Eddy Composite Properties

To determine the extent to which the presence of the Madagascar Ridge also influences the eddy properties, we analyzed the radial distribution of the eddy properties from the eddy composite, computed as outlined in Section 2.1.5, for all identified eddies within the boxes mentioned above in the two simulation experiments. The results are presented in Figure 5.

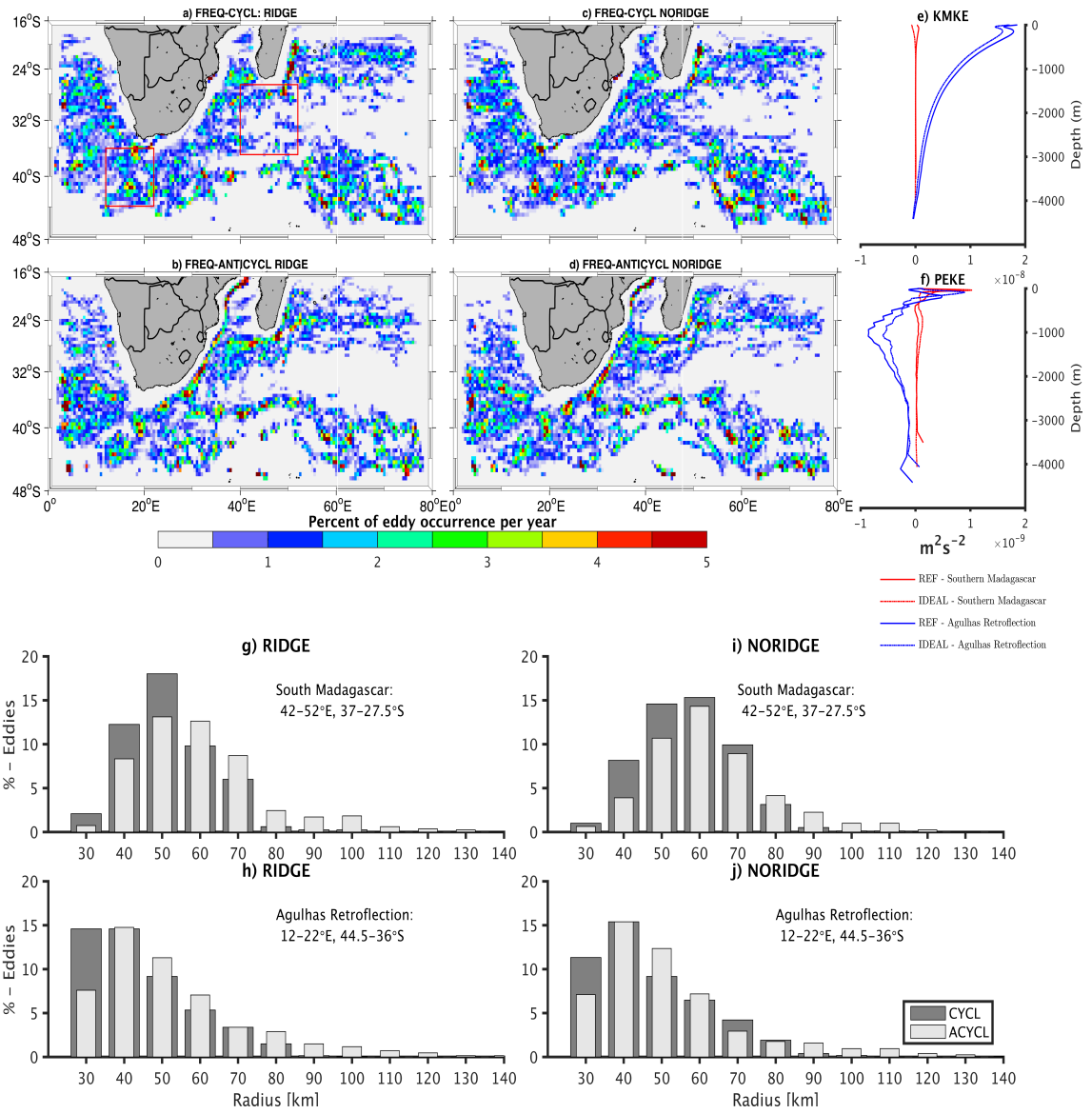**Figure 4.** Panels a) to d) show the distribution of the eddy frequency of occurrences per year, estimated in bins of $0.5° \times 0.5°$ for respectively cyclonic and anticyclonic eddies derived from the control experiment in panels a) and b), and from the idealized experiment in panels c) and d). The red boxes overlaid in panel a) mark the areas over the Madagascar Ridge and the Agulhas Retroflection area. The respective profiles of KmKe and PeKe energies are presented in panels e) and f). Finally, the histograms of eddy density distribution for the control experiment are shown in panels g) and h), and for the idealized experiment in panels i) and j).

Similar to Halo et al. (2014a), the distribution of each eddy structure amplitude (Figure 5-a, -d), follow a Gaussian distribution. Interestingly, both cyclonic and anticyclonic structures with radii smaller than 100 km have overlapping profiles (i.e. dots are superimposed on the lines) regardless of the experiment (control or idealized) and location (Madagascar Ridge domain or Agulhas Retroflection region). However departure between the dotted and continuous lines are observed for anticyclonic structures with radii of 100 km and larger. Note that the amplitude in the Agulhas Retroflection is greater than in the south of Madagascar region. The same is true for the distribution of the eddy azimuthal velocities (Figure 5-b, -e), the difference being that cyclonic eddy velocities in the idealized experiment were relatively smaller than in the control experiment for the region south of Madagascar (Figure 5-b).

Nevertheless, for all experiments it is apparent that a sharp slope exists in sea surface elevation which coincides with an extrema in azimuthal velocity at the edge of the eddy structures, consistent with the piece-wise distribution proposed by Castelão and Johns (2011).

A more distinct profile characterized by a flat plateau in the core of the eddies emerges when comparing the distribution of the relative vorticity in the two experiments (Figure 5-c, -f). In the Agulhas Retroflection region the flat plateau is observed in large anticyclonic structures in both idealized and control experiments (Figure 5 -f). This once again consolidate our finding that the excision of the Madagascar Ridge has no apparent impact on the eddy field in the Agulhas Retroflection region. However, in the region south of Madagascar the profiles for the large anticyclonic eddy structures differ. The profile is flat in the control experiment, and exponential in the idealized experiment, following similar distribution to that of smaller eddies (Radii < 100 km).

The emergence of a flat plateau in the core of larger anticyclonic structures followed by a sharp transition to an annulus of cyclonic vorticity is an indication of the presence of a second class of anticyclonic eddies (Castelão & Johns, 2011), commonly known as anticyclonic Rings. Note that Madagascar Rings were formed south of Madagascar only in the control experiment (i.e. when the Ridge was present). Similar ring structures have been observed in several ocean basins, as in the North Brazil Current (Castelão & Johns, 2011), in the Gulf Stream (Olson, 1991), in the Agulhas Current (Duncombe Rae, 1991; Pichevin et al., 1999), and in the Mozambique Channel (Halo et al., 2014a).

The ring properties for the different experiments and region can be further examined according to: (1) the capacity to trap material (a measure of nonlinearity) estimated from the ratio between the eddy rotational speed U_{rms} and the eddy translation speed C_{eddy}, $R_f = \frac{U_{rms}}{C_{eddy}}$ (Chelton et al., 2011); (2) the Rossby number (a measure of the eddy robustness), determined by the eddy relative vorticity ζ normalized by the eddy planetary vorticity f, $R_o = |\frac{\zeta}{f}|$ (Graves et al., 2006; Kurian et al., 2011); (3) the lifetime; and (4) estimation of the maximum distances traveled (Halo et al., 2014b). Their distribution per class of eddy radii is presented in the right panels of Figure 5.

In both experiments, the overall results (see Figure 5) suggest that the rings (Radii $\geq$ 100 km) were weakly nonlinear, unable to retain material in their core ($R_f < 1$, $R_o < 0.01$), in contrast to the classic eddy types (Radii < 100 km), (Figure 5-g,-h). The maximum travelled distance was 1003 km, and the maximum lifespan was 191 days (Figure 5-i). This suggests the rings generated south of Madagascar are sufficiently energetic to cross the Mozambique Basin, and interact with the oceanic environment in the vicinities of the Agulhas Current. On the other hand, the rings may not notably contribute to cross-basin material transports between the Mozambique and Natal Basins.
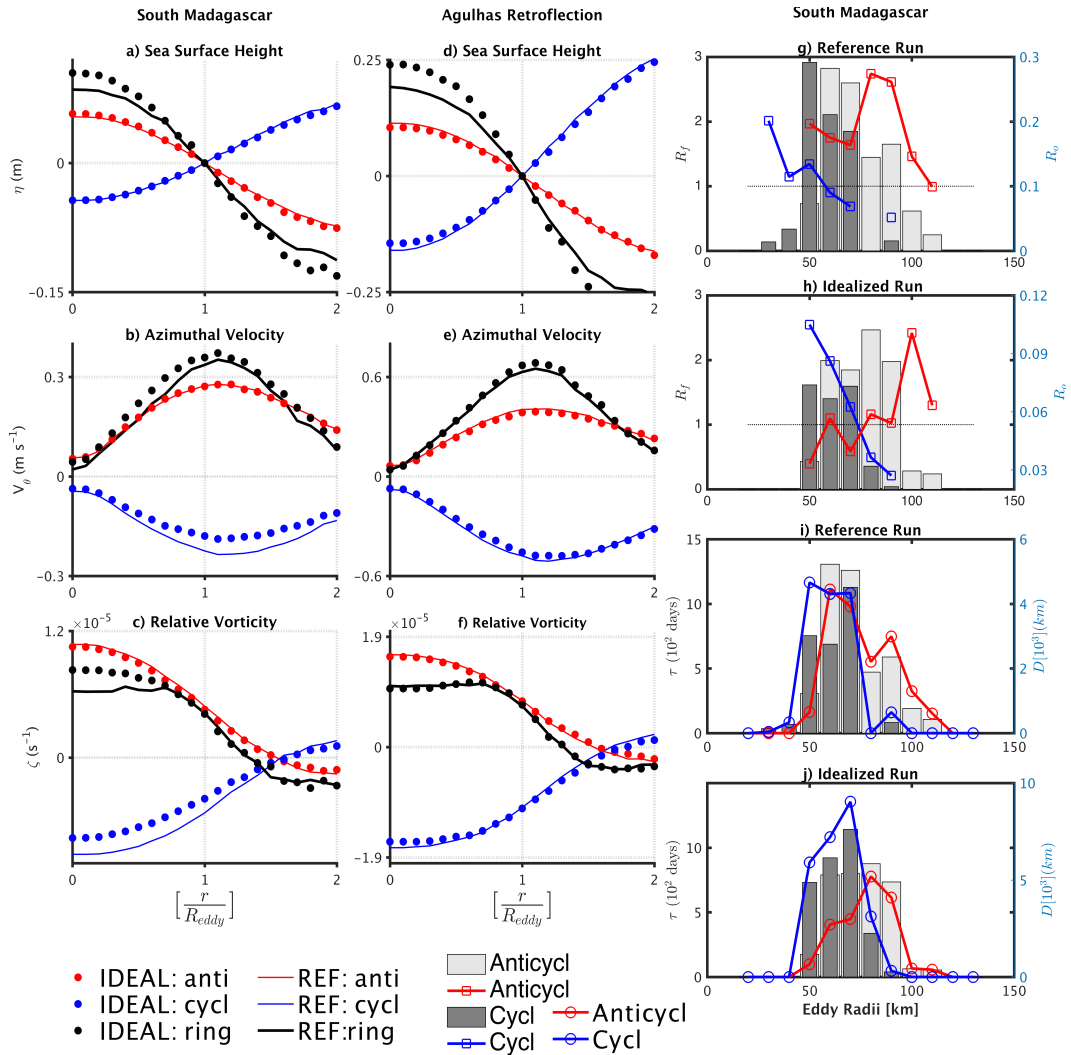
Figure 5. Eddy characteristics (model years 4 - 11) regarding the radial distribution of sea surface height (top panels a) and d)), azimuthal velocity (middle panels b) and e)), and vertical component of relative vorticity (lower panels c) and f)) as function of their distance from the eddies origin. Left panels represent eddies identified within the Madagascar Ridge domain (red boxes in Figure 4-a), the middle panels represent the red box in the Agulhas Retroflection area (Figure 4-a). Note that the vertical scales vary between the left and middle panels. The right panel represent histograms of size distribution of those eddies identified south of Madagascar region, as function of both eddy nonlinearity (R_f) and Rossby radius (R_o) in the control (g) and idealized experiment experiment (h), and lifetime (τ) and maximum travelled distance (D) in the control (i) and idealized experiment (j).

4 Conclusion

In this study we have carried out numerical model experiments under two distinctly different bathymetric configurations, characterized by the presence and absence of the Madagascar Ridge. In doing so the extent to which the Ridge influences the variability of the oceanic circulation in the greater Agulhas Current system has been examined leading to the following two main findings:

(1) The presence of the Madagascar Ridge controls volume transport with around ~ 10 Sv across the branches of the subtropical gyre of the southwestern Indian Ocean, namely, the southern extension of the South East Madagascar Current, the Agulhas Current, and the Agulhas Return Current.

(2) The presence of the Madagascar Ridge enhances the eddy formation in the region south of Madagascar, and excites the emergence of a secondary class of large (radii ≥ 100 km) anticyclonic eddies - "Madagascar rings", in addition to the classic eddy types. The Madagascar rings were formed south of Madagascar only in the control experiment (when the Ridge was present).

This study complements previous research in the region, and strengthen the understanding of the role that Madagascar Ridge plays for the regional oceanography.

Considering that a modelling framework with at least $1/32°$ grid resolution is required to adequately produce baroclinic instability (Hogan & Hurlburt, 2000), the use of nested grid configurations similar to that implemented in the Agulhas Current by Tedesco et al. (2019), might be more appropriate for a more comprehensive assessment of the role of Madagascar Ridge.

Data Availability Statement

The CROCO model code is freely available at $https://www.croco-ocean.org/$. The files containing eddies simulated in both control and idealized experiments are freely available at zenodo data repository with registered doi: $10.5281/zenodo.10971648$. The eddy detection toolbox can be freely assessed at zenodo software repository,at $https://zenodo.org/records/3862545$. version 2. It is described in detail in Halo et al. (2014a). Satellite altimetry data is freely available at $https://data.marine.copernicus.eu/product/$.

References

Anilkumar, N., Pednekar, S., & Sudhakar, M. (2007). Influence of ridges on hydrographic parameters in the South-West Indian Ocean. *Mar. Geophys. Res.*, *28*, 191-199. (doi: 10.1007/S11001-007-9026-5)

AVISO. (2015). Ssalto duacs user handbook. (M)SLA and (M)ADT near-real time and delayed time products. *Ssalto. Duacs.*, *4rev 4*. (doi: CLS-DOS-NT-06-034)

Beal, M. L., & Bryden, H. L. (1999). :The velocity and vorticity structure of the Agulhas Current at $32^c irc$S. *J. Geophys. Res.*, *104*, 5151 - 5171.

Biastoch, A., Böning, C. W., Schwarzkopf, F. U., & Lutjeharms, J. R. E. (2009). Increase in Agulhas leakage due to poleward shift of Southern Hemisphere westerlies. *Nature*, *462*, 495-498. (doi:10.1038/nature08519)

Bryden, H. L., Beal, L. M., & Duncan, L. M. (2005). Structure and transport of the Agulhas Current and its temporal variability. *J. Phys. Oceanogr.*, *61*, 479-492.

Castelão, G. P., & Johns, W. E. (2011). Sea surface structure of north brazil current rings derived from shipboard and moored acoustic doppler current profiler observations. journal of geophysical research. *J. Geophys. Res.*, *116*, CO1010. (doi:10.1029/2010JC006575)

Chelton, D. B., deSzoeke, R. A., Schlax, M. G., Naggar, K. E., & Siwertz, N. (1998). Geographical variability of the first-baroclinic rossby radius of deformation. *J. Phys. Oceanogr.*, *28*, 433-460.

Chelton, D. B., Schlax, M. G., & Samelson, R. M. (2011). Global observations of nonlinear mesoscale eddies. *Prog. Oceanog.*, *91*, 167-216. (doi:10.1016/j.pocean.2011.01.002)

Da Silva, A. M., Young, C. C., & Levitus, S. (1994). *Atlas of surface marine data 1994, vol. 1, algorithms and procedures* (Tech. Rep.). U. S. Department of Commerce, NOAA.

De Ruijter, W. P. M., Ridderinkhof, H., Lutjeharms, J. R. E., Schouten, M. W., & Veth, C. (2002). Observations of the flow in the Mozambique Channel. *Geophys. Res. Lett.*, *29*, 1401-1403.

De Ruijter, W. P. M., van Aken, H. M., Beier, E. J., Lutjeharms, J. R. E., Matano, R. P., & Schouten, M. W. (2004). Eddies and dipoles around South Madagascar: formation, pathways and large-scale impact. *Deep Sea Res., Part I*, *51*, 383-400. (doi: 10.1016/j.dsr.2003.10.011)

Donohue, K. A., Firing, E., & Beal, L. (2000). Comparison of three velocity sections of the Agulhas Current and Agulhas Undercurrent. *J. Geophys. Res.*, *105*, 585-593.

Donohue, K. A., & Toole, J. M. (2003). :A near synoptic survey of the SouthWest Indian Ocean. *Deep Sea Res., Part II*, *50*, 1893-1931.

Duncombe Rae, C. M. (1991). Agulhas retroflection rings in the South Atlantic Ocean: an overview. *S. Afr. J. mar. Sci.*, *11(1)*, 327-344. (doi: 10.2989/025776191784287574)

Graves, L. P., McWilliams, J. C., & Montgomery, M. T. (2006). Vortex evolution due to straining: a mechanism for dominance of interior anticyclones. *Geophys. Astroph. F. Dyn.*, *100:3*, 151-183.

H., R., & De Ruijter, W. P. M. (2003). Moored current observations in the Mozambique Channel. *Deep Sea Res., Part II*, *50*, 1933-1955. (doi: 10.1016/S0967-0645(03)00041-9)

Halo, I., Backeberg., B., Penven., P., Ansorge., I., Reason, C., & Ullgren, J. E. (2014a). Eddy properties in the Mozambique Channel: A comparison between observations and two numerical ocean circulation models. *Deep Sea Res., Part II*, *100*, 38-53. (doi: 10.1016/j.dsr2.2013.10.15)

Halo, I., Penven., P., Backeberg., B., Ansorge., I., Shillington, F., & Roman, R. (2014b). Mesoscale eddy variability in the southern extension of the East

Madagascar Current: Seasonal cycle, energy conversion terms, and eddy mean properties. *J. Geophys. Res.*, *119*, 7324-7356. (doi: 10.1002/2014JC009820)

Harris, S., Noyon, M., Marsac, F., Vianello, P., & Roberts, M. (2020). Ichthyoplankton assemblages at three shallow seamounts in the South West Indian Ocean. *Deep Sea Res., Part II*, *176*, 104809. (doi: https://doi.org/10.1016/j.dsr2.2020.104809)

Herbette, S., Morel., Y., & Arham, M. (2003). Erosion of a surface vortex by a seamount. *jpo*, *33*, 1,664-1,679.

Hogan, P., & Hurlburt, H. (2000). Impact of Upper Ocean - Topographical coupling and isopycnal outcropping in japan/east sea models with 1/8 to 1/64 resolution. *jpo*, *30*, 2535-2561.

Kundu, P. K. (1990). *Fluid Mechanics* (Vol. 1). Academic. Press. (638pp)

Kurian, J., Colas, F., Capet, X., McWilliams, J. C., & Chelton, D. B. (2011). Eddy properties in the California Current System. *J. Geophys. Res.*, *116*, C08027. (doi:10.1029/2010JC006895)

Le-Bars, D., Durgadoo., J., Dijkstra., H., Biastoch, A., & de-Ruijter, W. (2014). An observed 20-year timeseries of Agulhas leakage. *Ocean Sci.*, *10*, 601-609. (doi: 10.5194/os-10-601-2014)

Loveday, B., Durgadoo., J. V., Reason., C., Biastoch., A., & Penven, P. (2014). Decoupling of the agulhas leakage from the Agulhas Current. *J. Phys. Oceanogr.*, *44 (7)*. (doi.org: 10.1175/JPO-D-093.1)

Marchesiello, P., McWilliams, J. C., & Shchepetkin, A. (2003). Equilibrium structure and dynamics of the California Current System. *J. Phys. Oceanogr.*, *33*, 753-783.

Marsac, F., Galletti, F., Ternon, J.-F., Romanov, E., Demarcq, H., Corbari, L., . . . Ménard, F. (2020). Seamounts, plateaus and governance issues in the southwestern indian ocean, with emphasis on fisheries management and marine conservation, using the Walters Shoal as a case study for implementing a protection framework. *Deep Sea Res., Part II*, *Topical Studies in Oceanography*, *176*, 104715. (doi: https://doi.org/10.1016/j.dsr2.2019.104715)

Matano, R. P., Simionato, & Strub, P. T. (1999). Modeling the Wind-Driven Variability of the South Indian Ocean. *J. Phys. Oceanogr.*, *29*, 217-230.

Nairn, A. M., & Stehli, F. (1982). *The ocean basins and margins: Volume 6 the indian ocean.* New York: Plenum Press.

Nauw, J. J., van Aken, H. M., Webb, A., Lutjeharms, J. R. E., & Ruijter, W. P. M. D. (2008). Observations of the southern East Madagascar Current and Undercurrent and Countercurrent system. *J. Geophys. Res.*, *113*, C08006. (doi:10.1029/2007JC004639) doi: 10.1029/2007JC004639

Olson, D. (1991). Rings in the ocean. *Ann. Rev. Earth Planet. Sci.*, *19*, 283-311.

Palastanga, V., van Leeuwen, P. J., & Ruijter, W. P. M. D. (2006). A link between low-frequency mesoscale eddy variability around Madagascar and the large-scale Indian Ocean variability. *J. Geophys. Res.*, *111*, C09029. (doi:10.1029/2005JC003081)

Parson, L. M., & Evans, A. J. (2005). Seafloor topography and tectonic elements of the Western Indian Ocean. *Philos. Trans. R. Soc. London A*, *363*, 15-24. (doi: 10.1098/rsta.2004.1472)

Penven, P., Échevin, V., Pasapera, J., Colas, F., & Tam, J. (2005). Average circulation, seasonal cycle and mesoscale dynamics of the Peru Current System: a modeling approach. *J. Geophys. Res.*, *110*. (C10021, doi: 10.1029/2005JC002945)

Penven, P., Marchesiello, P., Debreu, L., & Lefèvre, J. (2008). Software tools for pre- and post-processing of oceanic regional simulations. *Env. Model. Soft.*, *23*, 660-662. (doi:10.1016/j.envsoft.2007.07.004) doi: 10.1016/j.envsoft.2007.07.004

Percival, D. B., & Walden, A. T. (1993). Spectral Analysis for Physical Applications: Multitaper and Conventional Univariety Techniques. *Cambridge.*

Press..

Pichevin, T., Nof, D., & Lutjeharms, J. R. E. (1999). Why are there Agulhas rings? *J. Phys. Oceanogr.*, *29*, 693-707.

Pollard, R., & Read, J. (2017). Circulation, Stratification and seamounts in the Southwest Indian Ocean. *Deep Sea Res., Part II*, *Topical Studies in Oceanography, 136*, 36-43. (doi:10.1016/j.dsr2.2015.02.018)

Quartly, G. D., Buck, J. J. H., Srokosz, M. A., & Coward, A. C. (2006). Eddies around Madagascar - The Retroflection re-considered. *J. Mar. Sys.*, *63*, 115-129. (doi:10.1016/j.jmarsys.2006.06.001) doi: 10.1016/j.jmarsys.2006.06.001

Read, J., & Pollard, R. (2017). An introduction to the physical oceanography of six seamounts in the southwest Indian Ocean. *Deep Sea Res., Part II*, *Topical Studies in Oceanography, 136*, 44-58. (doi:10.1016/j.dsr2.2015.06.022)

Ridderinkhof, W., Le Bars, D., A. S. von der Heydt., & De Ruijter, W. P. M. (2013). Dipoles of the South-east Madagascar Current. *Geophys. Res. Lett.*, *40*, 558-562. (doi:10.1002/grl.50157)

Ridgway, K. R. J. R. D., & Wilkin, J. L. (2002). Ocean interpolation by four-dimensional least squares-application to the waters around australia. *J. Atm. Ocean. Tech.*, *19*, 1357-1375.

Risien, C., & Chelton, D. B. (2008). A Global Climatology of Surface Wind and Wind Stress Fields from Eight Years of QuikSCAT Scatterometer Data. *J. Phys. Oceanogr.*, *38*, 2379-2413. (doi:10.1175/2008JPO3881.1)

Roberts, M., & Ternon, J.-F. (2020). The MADRidge project - a major contribution to IIOE2-WIOURI focusing on three shallow seamounts and their pelagic ecosystems in the vicinity of the Madagascar Ridge. *Deep Sea Res., Part II*, *176*, 104817. (doi: https://doi.org/10.1016/j.dsr2.2020.104817)

Roberts, M., Ternon., J.-F, Marsac., F., Noyon., M., & Payne, A. (2020). The MADRidge project: Bio-physical coupling around three shallow seamounts in the South West Indian Ocean. *Deep Sea Res., Part II*, *176*, 104813. (doi: https://doi.org/10.1016/j.dsr2.2020.104813)

Rouault, M., Penven, P., & Pohl, B. (2009). Warming in the Agulhas Current system since the 1980's. *Geophys. Res. Lett.*, *36*, L12602. (doi:10.1029/2009GL037987)

Royer, T. C. (1978). Ocean eddies gener- ated by seamounts in the north pacific. *Science*, *199*, 1,063-1,064.

Schott, F. A., Fieux, M., Kindle, J., Swallow, J., & Zantopp, R. (1988). The boundary currents east and north of Madagascar: 2 Direct measurements and model comparisons. *J. Geophys. Res.*, *93*, 4963 - 4974.

Schouten, M. W., De Ruijter, W. P. M., & van Leeuwen, P. J. (2002a). Upstream control of Agulhas ring shedding. *J. Geophys. Res.*, *107*, C83109. (doi: 10.1029/2001JC000804)

Schouten, M. W., De Ruijter, W. P. M., van Leeuwen, P. J., & Ridderinkhof, H. (2003). Eddies and variability in the Mozambique Channel. *Deep Sea Res., Part II*, *50*, 1987-2003. (doi: 10.1016/S0967-0645(03)00042-0)

Shchepetkin, A. F., & McWilliams, J. C. (2005). The regional oceanic modeling system (ROMS): a split-explicit, free-surface, topography-following-coordinate oceanic model. *Ocean Model.*, *9*, 347-404. (doi: 10.1016/j.ocemod.2004.08.002)

Siedler, G., Rouault, M., Biastoch, A., Backeberg, B., Reason, C. J. C., & Lutjeharms, J. R. E. (2009). Modes of the southern extension of the East Madagascar Current. *J. Geophys. Res.*, *114*, C01005. (doi: 10.1029/2008JC004921)

Stramma, L., & Lutjeharms, J. R. E. (1997). The flow field of the subtropical gyre in the South Indian Ocean into the Southeast Atlantic Ocean: A case study. *J. Geophys. Res.*, *99*, 14053 - 14070.

Swallow, J., Fieux, M., & Schott, F. A. (1988). :The boundary currents east and north of Madagascar 1: Geostrophic currents and transports. *J. Geophys.*

672   *Res.*, *93*, 4951 - 4962.

673   Swart, S., S. Speich., Ansorge, I., Goni, G., Gladyshev, S., & Lutjeharms, J.   (2008).

674   :Transport and Variability of the Antarctic Circumpolar Current south of

675   South Africa.   *J. Geophys. Res.*, *113*, C09014.   (doi:10.1029/2007JC004223)

676   doi: 10.1029/2007JC004223

677   Tedesco, P., Gula, J., Ménesguen, C., Penven, P., & Krug, M. (2019). Generation of

678   Submesoscale Frontal Eddies in the Agulhas Current.   *J. Geophys. Res.*, *124*,

679   7606-7625. (doi: https://doi.org/10. 1029/2019JC015229)

680   Thompson, D. J. (1982). Spectrum estimation and harmonic analysis. *Proc. IEEE.*,

681   *70*, 1055-1096. (doi:10.1109/proc.1982.12433)

682   van Sebille, E., Barron, C. N., Biastoch, A., van Leeuwen, P. J., Vossepoel, F. C.,

683   & De Ruijter, W. P. M.   (2009b).   Relating Agulhas Leakage to the Agul-

684   has Current retroflection location.   *Ocean Sci.*, *5*, 511-521.   (www.ocean-

685   sci.net/5/511/2009)

686   van Sebille, E., Biastoch, A., van Leeuwen, P. J., & De Ruijter, W. P. M. (2009a). A

687   weaker Agulhas Current leads to more Agulhas leakage.   *Geophys. Res. Lett.*,

688   *36*, L03601. (doi:10.1029/2008GL036614)

689   Vianello, P., Herbette, S., Ternon, J., Demarcq, H., & Roberts, M.   (2020b).

690   Observation of a mesoscale eddy dipole on the northern Madagas-

691   car Ridge: consequences for the circulation and hydrography in

692   the vicinity of a seamount.   *Deep Sea Res., Part II*, *176*, 104815.

693   (https://doi.org/10.1016/j.dsr2.2020.104815)

694   Vianello, P., Ternon, J., Demarcq, H., Herbette, S., & Roberts, M.   (2020a).   Ocean

695   currents and gradients of surface layer properties in the vicinity of the mada-

696   gascar ridge (including seamounts) in the South Western Indian Ocean.   *Deep*

697   *Sea Res., Part II*, *176*, 104816. (https://doi.org/10.1016/j.dsr2.2020.104816)